Chapter 2

A new series of thiazole-based gelators and its potential application

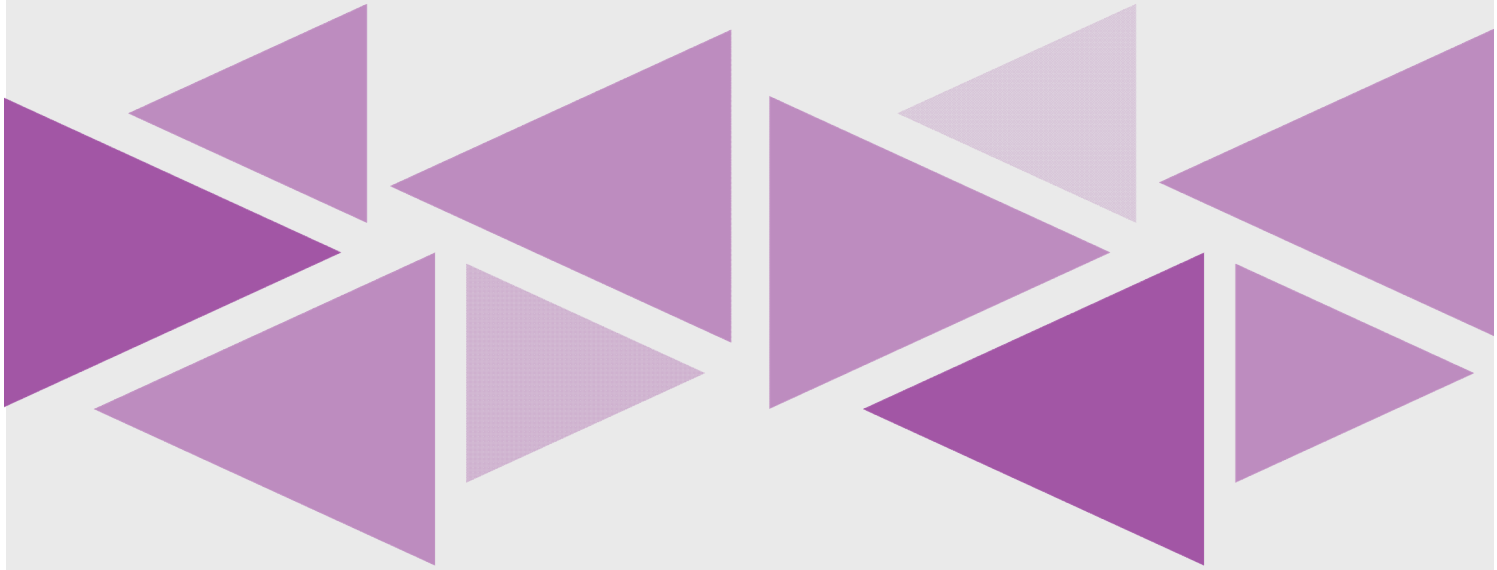

2.1 Introduction

LMWGs stands for Low Molecular Weight gelators, typically with low molecular mass (<3000 Da.) are the class of molecules which immobilize the solvent at very low concentration[1–5]. LMWGs are getting quite popular due to their applications in anion sensing[6], drug delivery[7], pollutant remediation[8,9], electrochromic materials[10], and many more. One of the major impediments in designing a new LMWGs are the structural diversity of known molecules with gelation properties such as metallogel[6], dendritic[11], nucleobases[12], sugar[13] and π-systems[14], etc. Another challenge in designing new LMWGs is the presence of supramolecular polymorphism in various hydrogen bonding functional groups such as Urea[15], Thiourea[16], Amide[17,18], which makes the prediction of hydrogen bonded network of molecule in the gel network extremely difficult.

As evident from the majority of work that it is extremely difficult to predict the ability of molecules to gel a solvent (organic/aqueous) beforehand based on its molecular structure[19]. Therefore, some of the major challenges in this area is to design, synthesis, and to find application of LMWGs and to understand the probable mechanism of gelation and to explore the link between the molecular packing, supramolecular assembly of molecular fibers and three-dimensional (3-D) macroscopic network leading to gelation behaviour[20].

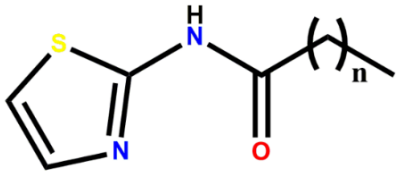

Where n=9, 10, 11, 12, 13, 14, 15, 16
Tz-9, 10, 11, 12, 13, 14, 15, 16

Scheme 2.1 *List of compounds used in the present study (synthesis, characterization, gelation properties of compounds (Tz-10 to Tz-16) are reported earlier[21].*

To address the problem in hand, we decided to synthesize a new class of compounds that may form metastable gel in solvents and in suitable condition may be crystallized. This approach leads to discovery of new gelators and significantly improved our understanding of the mechanism of the formation of physical gels. In this endeavor, we serendipitously obtained versatile supramolecular gels based on thiazole moiety (amides[21,22], salts[23], metallogel[24]). Interestingly, gelation property of long chain aliphatic amides of thiazole moiety was found to depend upon the number of methylene

groups in the aliphatic backbone i.e., odd-even effect. Despite various efforts by us and other[25] couldn't provide a conclusive explanation for the odd-even effect in these series of thiazole amides based gelators. Therefore, in the present work, we synthesized a new and known thiazole based aliphatic amides (**Scheme 1**) to understand the hierarchal assembly of molecules in the solid-state to metastable gel state. Interestingly, from the list of compounds, Tz-9 displayed well-defined packing even in the solid-state when analysed using SAXS (Small Angle X-ray Scattering) and SANS (Small Angle Neutron Scattering). Therefore, we decided to direct our effort to establish the relationship between packing of Tz-9 in solid-state (SANS, Powder and single crystal X-ray study) and supramolecular assembly in gel state (variable temperature SANS study). Moreover, Tz-9 displayed excelled selectivity and sensitivity towards fluoride ion.

2.2 Materials and Physical measurements

2.2.1 Materials

Long chain aliphatic carboxylic acids and 2-aminothiazole were purchased from Sigma Aldrich. Oxalyl chloride and triethylamine were obtained from CDH (P) Ltd., India and used without any further purification. Solvents for gelation studies was reagent grade and used without any distillation, Further solvents for synthesis was purified and dried over molecular sieve.

2.2.2 NMR Spectroscopy

NMR spectra of Compound was recorded in $CDCl_3$ on BRUKER ADVANCE, 400MHz Spectrometer at 258 kelvin temperature.

2.2.3 FT-IR Spectroscopy

FT-IR Studies of Tz-9 and its xerogel were performed in solid-state using KBr pellet on BRUKER ALPHA FT-IR Spectrometer and spectra were recorded in the wavenumber range from 400-4000 cm^{-1}.

2.2.4 Polarized optical Microscope

Supersaturated gelator solution was placed on glass slide and allow to cool down at room temperature to form gel and this gel was directly observed and images were taken using Leica DM 2500P Polarising optical microscope provided with the Linkam heating stage.

2.2.5 SEM Measurements

Hot solution of gelator in respective solvents was placed on sample holder and allowed to cool to form gel, and then dried under vacuum. Dried gel was subjected to gold sputtering using POLARON SC7620 Sputter Coater and this gold coated dried gel was subjected to JEOL JSM 5610 LV SEM instrument after carbon coating.

2.2.6 Hirshfeld Surface Calculations

The Hirshfeld surface calculations were performed by employing CrystalExplorer-17.5 Program[26].

2.2.7 Powder X-ray Diffraction

Powder XRD pattern of the neat gelator (Bulk) and xerogel (obtain from slow evaporation) was obtained from X'pert Pan Analytical Powder diffractometer with Cu KR (1.54 Å) radiation (45 kV, 40 mA). The proportional counter detector collected over the range of 2θ=10-50°.

2.2.8 Single crystal X-ray Diffraction (SCXRD)

Single crystal X-ray study was carried out on Single Crystal X-ray diffractometer (Xcalibur, EOS, Gemini diffractometer). All structures were solved and refined using the OLEX2[27] software and SHELXL[28,29] refinement package Graphics are generated using MERCURY 4.2.0. the structure of Tz-9 was solved by direct methods and refined in a routine manner. Non-hydrogen atoms were treated anisotropically. Whenever possible, the hydrogen atoms were located on a difference Fourier map and refined. In other cases, the hydrogen atoms are geometrically fixed.

2.2.9 UV-Visible Spectroscopy studies

The electronic spectra (in THF at room temperature) in the range of 200-600 nm were recorded on a model JASCO 7600 UV-VIS spectrophotometer.

2.2.10 Fluorescence study

Fluorescence spectra were recorded on a JASCO FP-6300 fluorescence spectrophotometer.

2.2.11 Small angle X-ray scattering (SAXS)

SAXS measurements were carried out using Anton Paar SAXSpace instrument which employs line collimated sealed tube X-ray source (Cu-Kα, λ = 0.1542 nm) operated at 40 kV, 50mA. The scattering intensities were monitored in transmission geometry using a 2D CCD detector (pixel size 24 micron) to the span of q (momentum transfer) range of 0.01 $Å^{-1}$ to 0.65 $Å^{-1}$. The sample holder is positioned at a distance of 305 mm from the CCD detector. The detector is operated at -40 °C to reduce the thermal noise. The collimation system, sample chamber, and beam path were enclosed in vacuum at a pressure below 3 mbar. A semi-transparent beam stop is employed to measure transmittance and zero q position. The data were processed using standard protocols. Instrumental smearing was considered during data analysis using the measured beam profile.

2.2.12 Small angle neutron studies (SANS)

SANS experiments were performed at the SANS diffractometer at Guide Tube Laboratory, Dhruva Reactor, Bhabha Atomic Research Centre, Mumbai, India[30]. In SANS, one measures the coherent differential scattering cross-section (dΣ/dΩ) per unit volume as a function of wave vector transfer Q (= 4π sinθ/λ, where λ is the wavelength of the incident neutrons and 2θ is the scattering angle). The mean wavelength of the monochromatized beam from neutron velocity selector is 5.2 Å with a spread of Δλ/λ ~ 15%. The angular distribution of neutrons scattered by the sample is recorded using a 1 m long one-dimensional He^3 position sensitive detector. The instrument covers a Q-range of 0.014–0.3 $Å^{-1}$. The powder and gel samples were contained in the quartz cell with 2 mm path length. Deuterated Acetonitrile is used for contrast to make the gel sample. The data have been analyzed by comparing the scattering from different models to the experimental data[31,32].Throughout the data analysis, corrections were made for instrumental smearing, where the calculated scattering profiles smeared by the appropriate resolution function to compare with the measured data. The fitted parameters in the analysis were optimized using a non- linear least-square fitting program to the model scattering. The modelling of the SANS data is described as follows,

The differential scattering cross-section per unit volume ($d\Sigma/d\Omega$) as measured for a system of monodisperse particles in a medium can be expressed as[33,34]

$$\left(\frac{d\Sigma}{d\Omega}\right)(Q) = nV^2\left(\rho_p - \rho_s\right)^2 P(Q)S(Q) + B \qquad \ldots\ldots\ldots\ldots\ldots\ldots (1)$$

where n denotes the number density of particles, ρ_p and ρ_s are, respectively, the scattering length densities of particle and solvent and V is the volume of the particle. $P(Q)$ is the intraparticle structure factor and $S(Q)$ is the interparticle structure factor. B is a constant term representing incoherent background, which is mainly due to the hydrogen present in the sample.

Intraparticle structure factor $P(Q)$ is decided by the shape and size of the particle and is the square of single-particle form factor $F(Q)$ as determined by[35]

$$P(Q) = \langle |F(Q)|^2 \rangle \qquad \ldots\ldots\ldots\ldots\ldots\ldots (2)$$

For a spherical particle of radius R, $F(Q)$ is given by

$$F(Q) = 3\left[\frac{\sin(QR) - QR\cos(QR)}{(QR)^3}\right] \qquad \ldots\ldots\ldots\ldots\ldots\ldots (3)$$

For a cylindrical micelle of length $L = 2l$ and cross-sectional radius R,

$$P(Q) = \int_0^{\pi/2} \frac{\sin^2(Ql\ \cos\beta)}{Q^2 l^2\ \cos^2\beta} \frac{4J_1^2(QR\ \sin\beta)}{Q^2R^2\ \sin^2\beta} \sin\beta\ \mathrm{d}\beta \qquad \ldots\ldots\ldots\ldots\ldots\ldots (4)$$

where β is the angle between the axis of the rod and bisectrix. J_1 is the Bessel function of order unity.

The polydispersity in size distribution of particle is incorporated using the following integration

$$\frac{d\Sigma}{d\Omega}(Q) = \int \frac{d\Sigma}{d\Omega}(Q,R)\, f(R) dR + B \qquad \ldots\ldots\ldots\ldots\ldots\ldots (5)$$

where $f(R)$ is the size distribution of the vesicles and usually accounted by a log-normal distribution as given by

$$f(R) = \frac{1}{\sqrt{2\pi}R\sigma} \exp\left[-\frac{1}{2\sigma^2}\left(\ln\frac{R}{R_{med}}\right)^2\right] \qquad \ldots\ldots\ldots\ldots\ldots\ldots (6)$$

where R_{med} is the median value and σ is the standard deviation (polydispersity) of the distribution. The mean radius (R_m) is given by $R_m = R_{med} \exp(\sigma^2/2)$.

The data have been analyzed by comparing the scattering from different models to the experimental data[31,32,36]. Throughout the data analysis, corrections were made for instrumental smearing, where the calculated scattering profiles smeared by the appropriate resolution function to compare with the measured data. The fitted parameters in the analysis were optimized using nonlinear least-square fitting program to the model scattering.

2.3 Experimental Procedures

2.3.1 Gelation Studies

Gelation test of Tz-9 was carried by taking a weighted amount (10 mg) of powdered compound in the known amount of solvent (1 mL) in a sealed vial. The vial was heated in an oil bath/water bath until the compound was completely solubilized in the solvent. The solution was kept for 3 hours at RT (25 °C) and the resulted mixture was checked for their gelation behaviour by "Inverted test-tube method"[3]. Gel transition temperature (T_{gel}) was measured by "dropping ball method" in which small glass ball weighing 10 mg was carefully placed on top of the gel (1 mL) and this gel was heated gradually (0.5 °C per minute), the temperature at which glass ball reaches bottom noted as T_{gel} temperature. Each experiment is repeated at least 3 times to get the average T_{gel} value for a given solvent/gelator system.

2.3.2 Absorption studies

The stock solution of Tz-9 (6 **μ**M) was prepared and the stock solution with the concentration of 100 **μ**M of various anions (Tetrabutylammonium salts of Fluoride, bromide and dihydrogenphosphate) were prepared in Tetrahydrofuran (THF). The calculated amount of stock solution of anion was added to the 2.5 mL of Tz-9 solution to get the required concentration of anion to carry out spectroscopic titrations.

2.3.3 Emission studies

The stock solution of Tz-9 (6 **μ**M) was prepared and the stock solution with the concentration of 100 **μ**M Tetrabutylammonium fluoride (TBAF) were prepared in tetrahydrofuran (THF). The calculated amount of stock solution of TBAF was added to the 2.5 mL of compound-1 solution to get the required concentration of TBAF to carry out spectroscopic titrations.

2.3.4 Synthesis

Oxalyl chloride (1.5 equivalent) was added to the solution of fatty acid (1 equivalent) in dry dichloromethane with constant stirring at room temperature under the nitrogen atmosphere. After 12 hours, dichloromethane and excess oxalyl chloride were evaporated under reduced pressure. The undecanoyl chloride obtained after the reaction was dissolved in fresh dichloromethane and added slowly to the mixture of 2-aminothiazole (1 equivalent) and triethylamine (1.2 equivalent). The solution was stirred under nitrogen atmosphere for 18 hours. The reaction mixture was extracted with ethyl acetate, evaporated in high vacuum and purified by column chromatography over silica gel with 10% ethyl acetate: pet. ether eluent to get a yield of 62%.

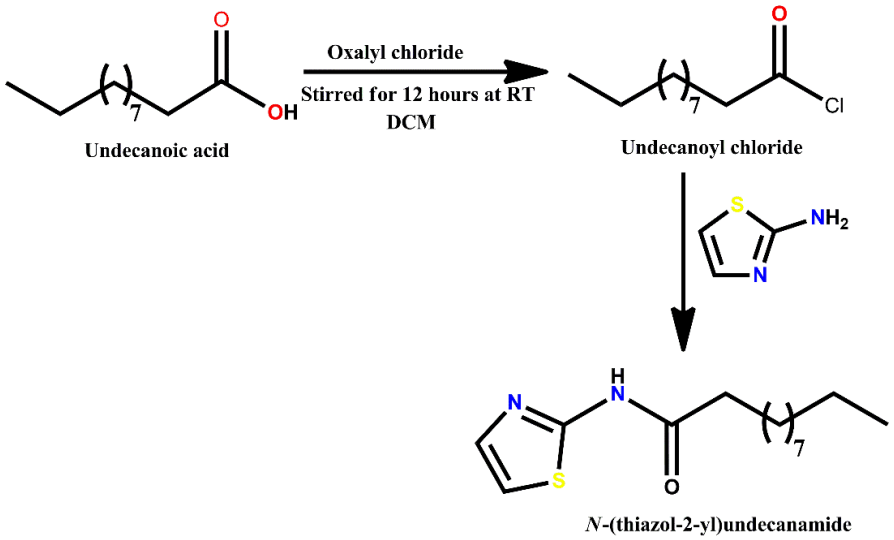

Scheme 2.2: *Preparation scheme for compound-1*

Analytical data

^{1}H NMR (400 MHz, $CDCl_3$, TMS): 11.347 (s, 1H, NH), 7.446 (d, 1 H; CH), 7.003 (d, 1H; CH), 2.560–2.552 (t, 2H; CH_2), 1.623–1.745 (m, 2H, CH_2), 1.424–1.269(m, 14H, CH_2), 0.908−0.891 (t, 3H; CH_3). MS (EI): m/z 268.418 $[M]^+$. FTIR (KBr): 3178, 2919, 2852, 1687, 1586, 1467, 1381, 1326, 1282, 1173, 1067, 960, 874, 809, 778, 719, 625, 520 cm^{-1}.

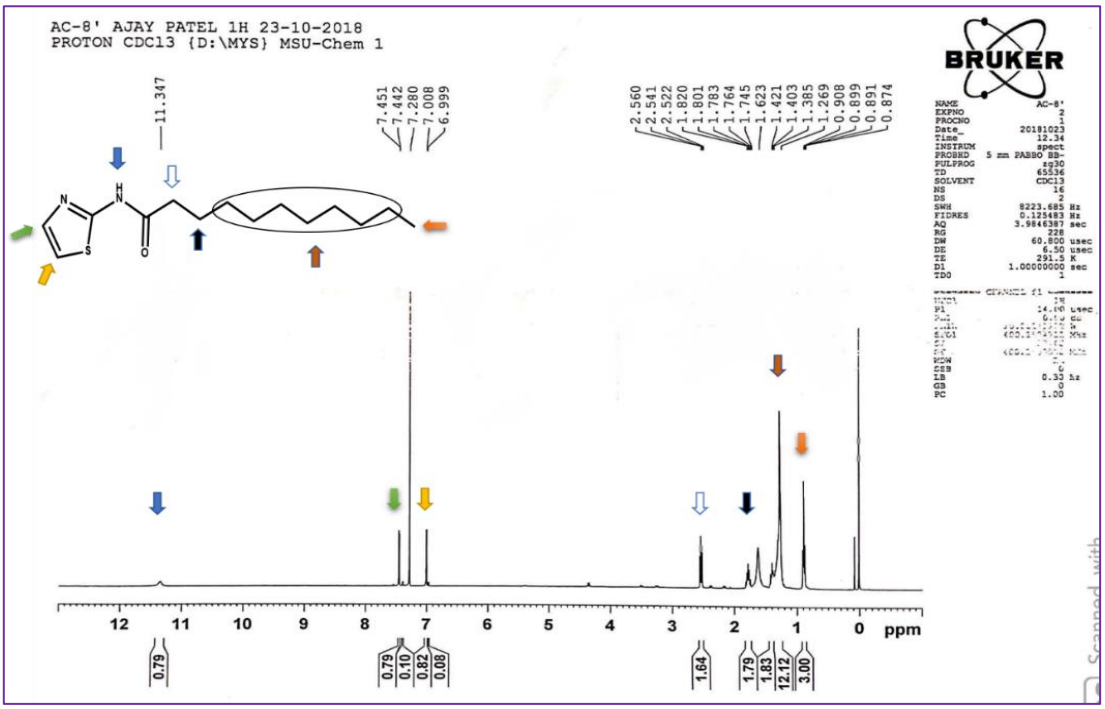

Figure 2.1 *^{1}H NMR spectrum of Tz-9 in $CDCl_3$(400 MHz)*

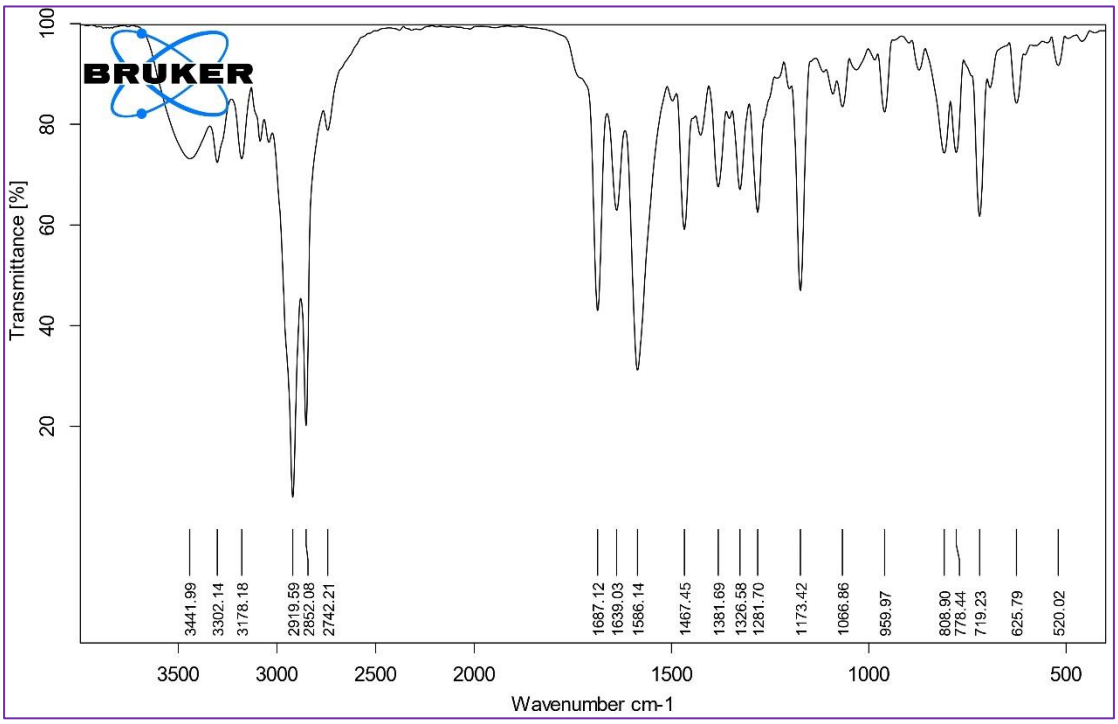

Figure 2.2 *IR spectra of TZ-9*

2.4 Results and Discussion

2.4.1 Gelation studies

Gelation studies of Tz-9 were performed on 25 solvents (polar and non-polar), summarized in table 2.1 and the formation of gel were verified using "Inverted tube method". The compound Tz-9 was found to gelate three different solvents (acetonitrile, methanol, propan-1,2-diol) and one commercial fuel (engine oil) effectively and were stable up to few months, except in the case of acetonitrile gel where crystal formation was observed after few days.

Table 2.1 *Gelation ability of Tz-9*

Solvent	mgc (%w/v)	T_{gel} (°C)
Acetonitrile	3.14	58
Methanol	6.29	63
Propan-1,2 diol	2.78	70
Engine oil	6.82	72
Chloroform	Soluble	-
Dichloromethane	Soluble	-
Acetone	Weak gel	-
Ethanol	Weak gel	-
DMF	Soluble	-
THF	Soluble	-
n-Hexane	Soluble	-
Diesel	Precipitate	-
Water	Precipitate	-
DMSO	Weak gel	-
1-hexanol	Weak gel	-
Octan-2-ol	Crystalized out	-
Isopropanol	Precipitate	-
1-Decanol	Precipitate	-
n-Decane	Soluble	-
3°Butanol	Soluble	-
1-Butanol	Soluble	-
Chlorobenzene	Soluble	-
Nitrobenzene	Soluble	-
Pyridine	Soluble	-

Interestingly, Tz-9 is able to gelate highly polar solvents such as Acetonitrile, Methanol and 1,2-Propanediol despite having a competitive hydrogen bonding site, i.e., amide functionality. Gels in different solvents were examined for their thermo-reversibility and minimum gelator concentration (mgc) of different solvents was determined to lie between 2.78-6.78 wt. % (w/v). The sol-gel temperature (T_{gel}) was determined using the dropping ball method and the effect of concentration of gelator on T_{gel} value was also determined (see Table 2.2).

The gradual increase in the value of T_{gel} with an increase in the concentration of gelator up to certain limiting value is well known in LMWGs study (Figure 2.3a). The higher value of T_{gel} with an increase in the concentration of gelator molecules may be attributed to an increase in fibrous network of molecules with better interconnectivity between fibers enhancing the stability.

Table 2.2 *Concentration based T_{gel} studies of* ***Tz-9***

Acetonitrile		Methanol		Prop-1,2-diol		Engine oil	
Conc. (% w/v)	T_{gel} (˚C)	Conc. (% w/v)	T_{gel} (˚C)	Conc. (% w/v)	T_{gel} (˚C)	Conc. (% w/v)	T_{gel} (˚C)
3.2	58	5	63	2.7	70	6.8	72
3.5	61	5.5	70	3	75	7.0	75
4.0	66	6.0	76	3.5	79	7.5	79
4.5	68	6.5	78	4.0	81	8.0	85
5.0	70	7.0	80	4.5	82	8.5	89
5.5	71	7.5	80	5.0	83	9.0	89
6.0	71	8.0	80	5.5	82	9.5	90

The plateau region of the curve suggests the saturation limit up to which molecules can be incorporated in the gel network. The thermodynamic parameter such enthalpy of melting (ΔH_m) was evaluated by using Schroder-van Laar equation (equation 7)[37,38].

$$\ln [\text{Gelator}] = \Delta H_m / RT_{gel} + \text{constant} \qquad (7)$$

The semi log plot of gelator concentration (in mole fraction) and $1/1000T_{gel}$ (K^{-1}) in four different solvents displayed linear relationship. (Figure 2.3b).

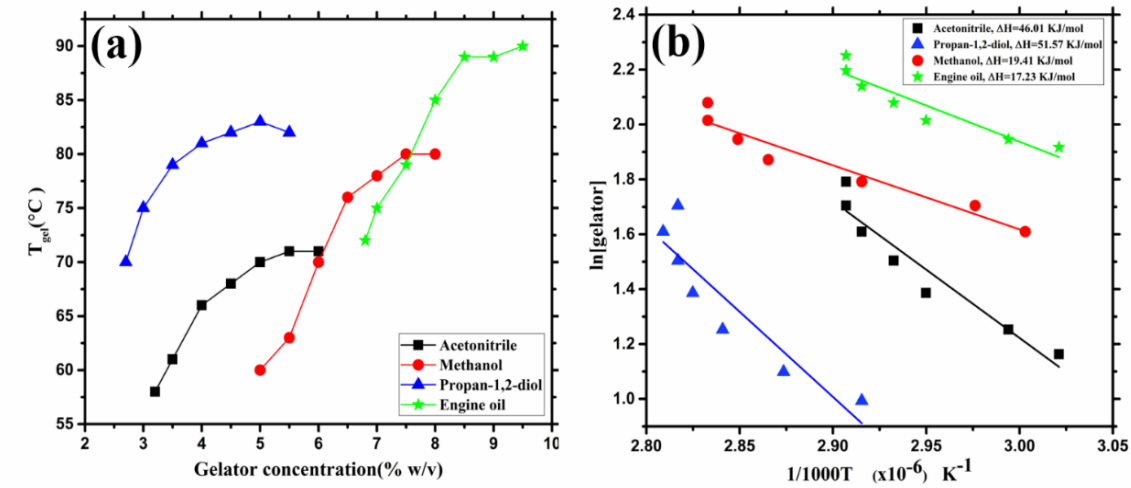

Figure 2.3 *(a)Plot of T_{gel} vs concentration of Tz-9 in Acetonitrile, Methanol, Propan-1,2-diol and Engine oil, (b)Linear plot of ln [Gelator] vs the reciprocal of T_{gel} of Tz-9*

The values of ΔH_m for Tz-9 in gelling solvents were found to be the smallest in the series of thiazole-amide based gelator for methanol and engine oil[21]. Understandably, the increase in the aliphatic chain of thiazole amide based gelator increases stability through interdigitation of alkyl chain and consequently, it reflects in the value of ΔH_m. Moreover, the values of ΔH_m for sol-gel transition of Tz-9 gelator in different solvents were found to lie between 17.5–92.7 kJ/mol, suggested a strong influence of solvents on melting of gelator fibers.

2.4.2 Morphological Studies

The morphological study of gelator fibers in xerogel was carried out using POM and SEM techniques. The optical micrographs of the gel fibers of **Tz-9** in different solvents are represented in Figure 2.4a-d. The well-defined needle shape crystalline fibers of **Tz-9** were observed in each optical micrograph in different solvents. The gel network in acetonitrile of **Tz-9** was further probed using SEM techniques. SEM micrographs of **Tz-9** in ACN (Figure 2.4e, f) displayed a well-defined rectangular shaped crystal with sharp edges and a flat surface. We would like to stress upon that 2-D micro-plate like morphology of xerogel are known in literature, even though a rare occurrence[39].

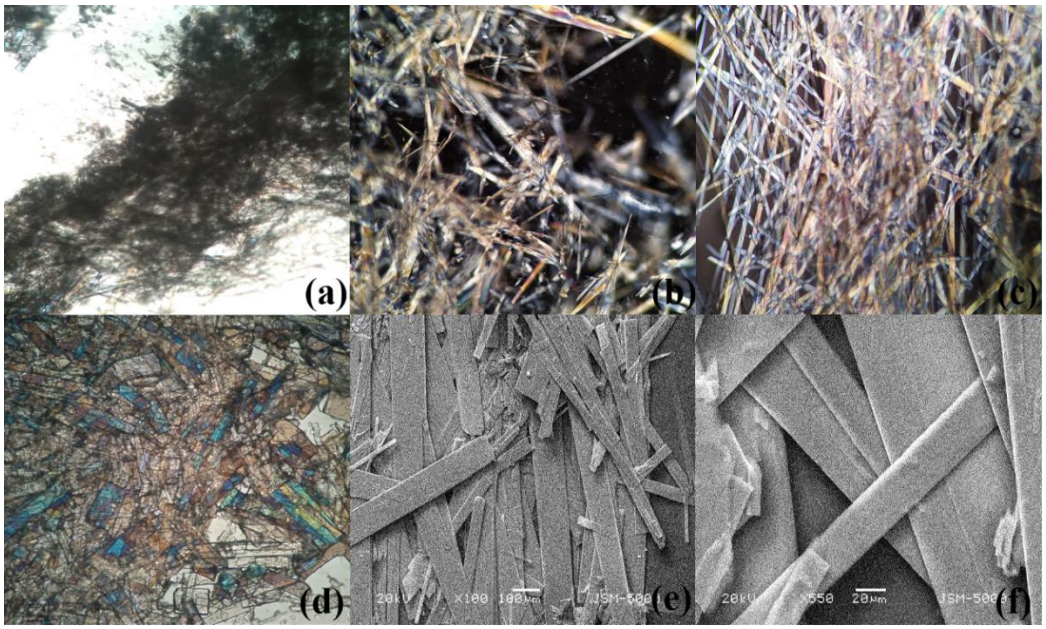

Figure 2.4 *POM images of gel obtained from Tz-9 at room temperature (a) Methanol, (b) Engine oil (c) Propane-1,2-diol (d) Acetonitrile (e, f) SEM image of Acetonitrile xerogel*

2.4.3 Infrared Studies

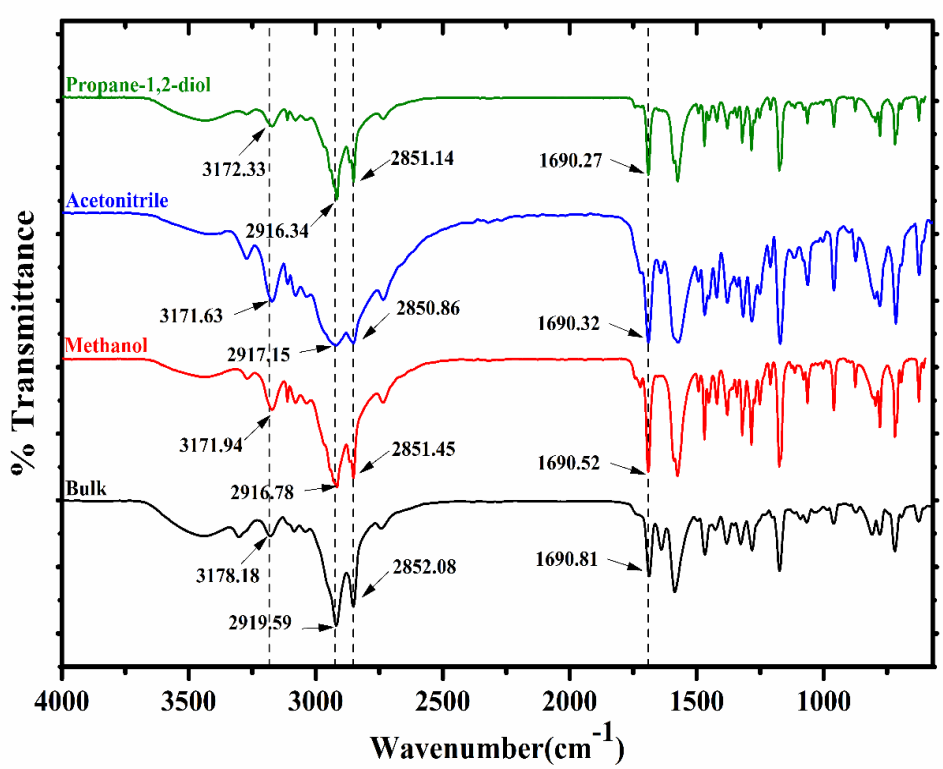

Figure 2.5 *IR Spectra of Tz-9 of bulk and xerogel obtained from various solvents.*

FT-IR spectroscopy technique was used for comparative study of the role of hydrogen bonding in the solid-state and xerogel state (dried gel) of Tz-9 in methanol, acetonitrile, 1,2-propanediol. (Figure 2.5). The solid-state IR of Tz-9 exhibits -N-H (amide) and C=O stretching frequencies at ~3178.18 and ~1690.81 cm^{-1}, respectively, Interestingly, C=O (carbonyl) frequency of amides was found to be unperturbed in solid state and in xerogels of Tz-9 in different solvents i.e., 1690 cm^{-1}, suggesting no change in hydrogen bonding pattern involving carbonyl functionality. Whereas, the shift of amine stretching frequency in solid state to xerogel state of Tz-9 may be attributed to the enhancement of hydrogen bonding between two different molecules of Tz-9. (see Figure 2.5). Moreover, symmetric and asymmetric stretching of the alkyl chain of Tz-9 (C–H group) at 2919 and 2852 cm^{-1} were due to alkyl chain trans zigzag conformation[40]. IR frequencies of C–H functionality of Tz-9 displayed no significant change (in solid and xerogel state) suggested the presence of alkyl chain interdigitation, unequivocally in all states.

2.4.4 Single crystal X-ray diffraction

Single crystal of **Tz-9** suitable for X-ray study was obtained from ACN gel after drying and its crystallographic date is summarized in Table 2.3. The **Tz-9** crystallized out in monoclinic $P2_1/c$ space group. The asymmetric unit contains one molecule of **Tz-9**(Figure 2.6).

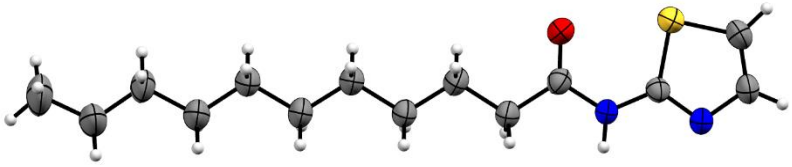

Figure 2.6 *Single crystal structure of Tz-9*

Table 2.3 *Crystallographic data of Tz-9*

Identification code	exp_1852
Empirical formula	$C_{14}H_{24}N_2OS$
Formula weight	267.40
Temperature/K	293
Crystal system	monoclinic
Space group	$P2_1/c$
a/Å	18.2738(12)
b/Å	4.9358(3)
c/Å	16.9344(16)
α/°	90
β/°	95.270(6)
γ/°	90
Volume/Å^3	1520.9(2)
Z	4
ρ_{calc}g/cm^3	1.168
F(000)	580.0
Crystal size/mm^3	0.543 × 0.137 × 0.02
Radiation	MoKα (λ = 0.71073)
2Θ range for data collection/°	6.28 to 58.428
Index ranges	$-24 \le h \le 24$, $-6 \le k \le 6$, $-21 \le l \le 21$
Reflections collected	17822
Independent reflections	3734 [R_{int} = 0.0625, R_{sigma} = 0.0622]
Data/restraints/parameters	3734/0/164
Goodness-of-fit on F^2	0.987
Final R indexes [I>=2σ (I)]	R_1 = 0.0575, wR_2 = 0.1501
Final R indexes [all data]	R_1 = 0.1181, wR_2 = 0.1953
Largest diff. peak/hole / e Å^{-3}	0.34/-0.23
CCDC No.	1973913

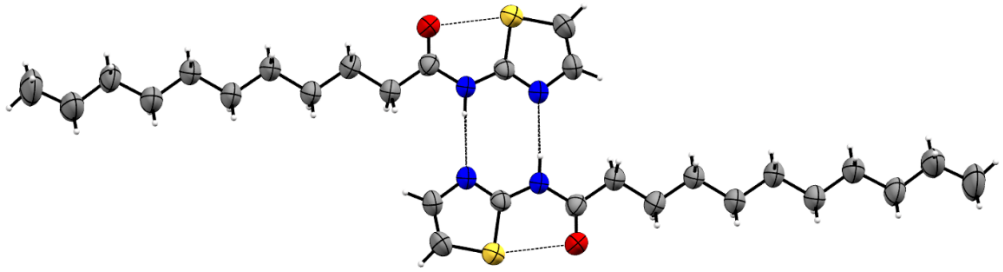

Figure 2.7 *Dimer motif form by two molecules of Tz-9*

The molecules of Tz-9 displayed hydrogen bonded supramolecular synthons such as cyclic N-H…N (N–H…N = 2.095 Å, ∟N–H…N = 173.27) and intramolecular S…O, consistent with other thiazole-based amides 21,22,41(Figure 2.7). Along with intramolecular hydrogen bonding the carbonyl (Figure 2.8) oxygen of amide of Tz-9 molecules are involved in bifurcated hydrogen bonding with neighbouring molecules (Figure 2.10). Interestingly, one C-H···O bond is within the plane of dimeric Tz-9 assembly, whereas the second C-H···O interaction is out of plane. The interplanar distance between the hydrogen-bonded assembly of Tz-9 is 3.59 Å. (C···O). The overall assembly may be compared with "brickwall motif"[41] or "molecular staircase"[42] (Figure 2.8).

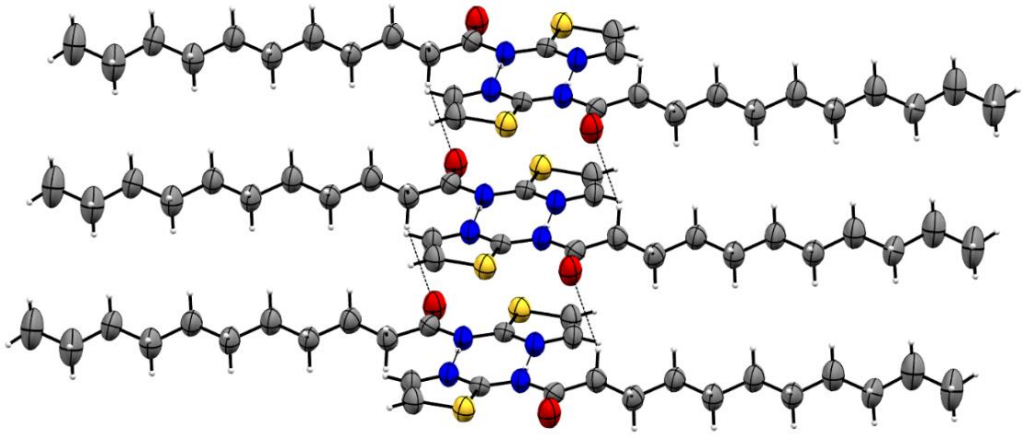

Figure 2.8 *"Molecular staircase" formed by dimer of Tz-9.*

Hirshfeld surface analysis[26] was carried out to get a quantitative idea about the contribution of non-covalent interactions on the overall packing of **Tz-9** molecules. Understandably, the contribution of van der Waals interaction was found to be a major governing force for packing along with a small contribution from various non-covalent interactions such as, S···H, O···S, H···O, N···H, etc. (Figure 2.9)

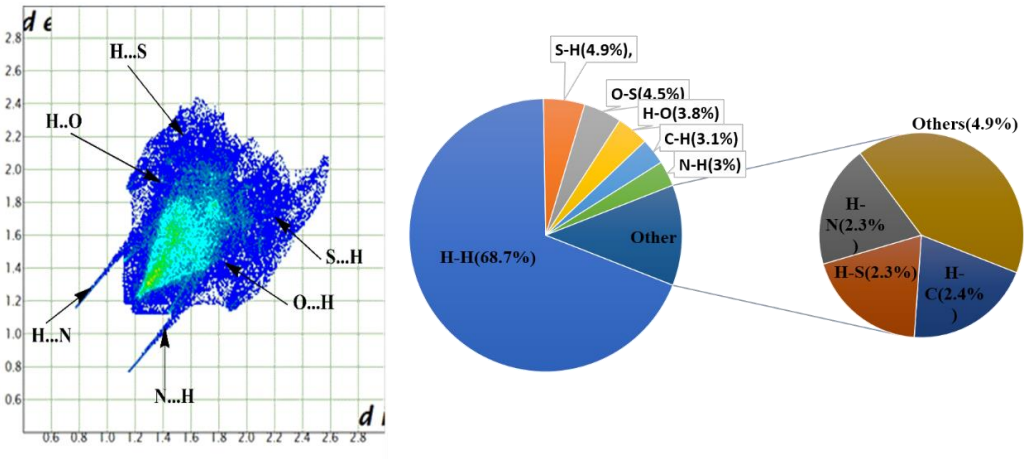

Figure 2.9 *2D fingerprint plot of Tz-9. The key interactions are marked with arrows and their percentage contribution is shown in pie chart.*

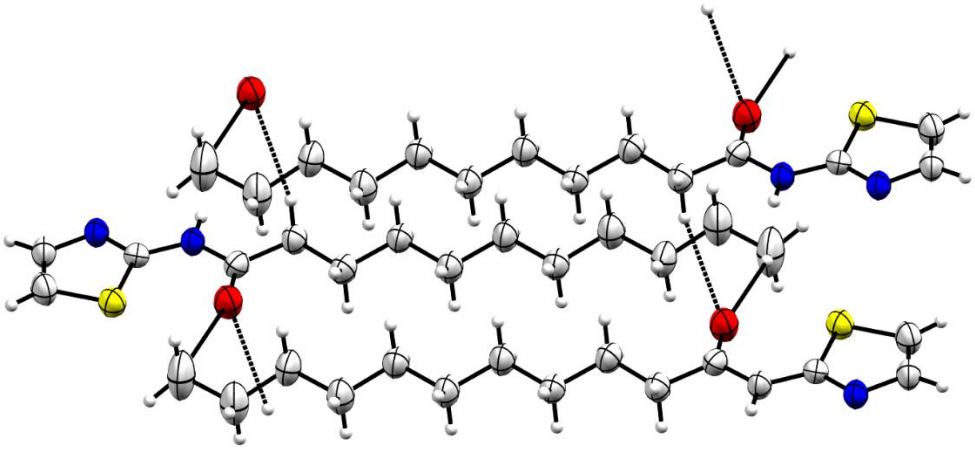

Figure 2.10 *Figure showing carbonyl oxygen of amide is involved in bifurcated hydrogen bonding*

2.4.5 Powder X-ray diffraction studies

PXRD pattern of **Tz-9** was recorded to get an insight in packing of molecules in xerogel (dried gel from acetonitrile) and compare it with the solid bulk and simulated powder XRD pattern obtained from single crystal structure of **Tz-9**, a well-established method to establish the packing of molecules at least in xerogel state[43]. As evident from the PXRD patterns of xerogel, simulated and bulk solid most of the peaks match well, especially, in case of bulk and xerogel (obtained from acetonitrile) (Figure 2.11). Interestingly, analysis of PXRD of bulk solid of Tz-9 revealed that d-values of four strongest peaks 17.4, 9.1, 6.0, and 4.5 Å, (Figure 2.12) approximately follow ratio of 1:1, 2:1, 3:1 and 4:1, respectively, suggesting a layered structure[44–46].

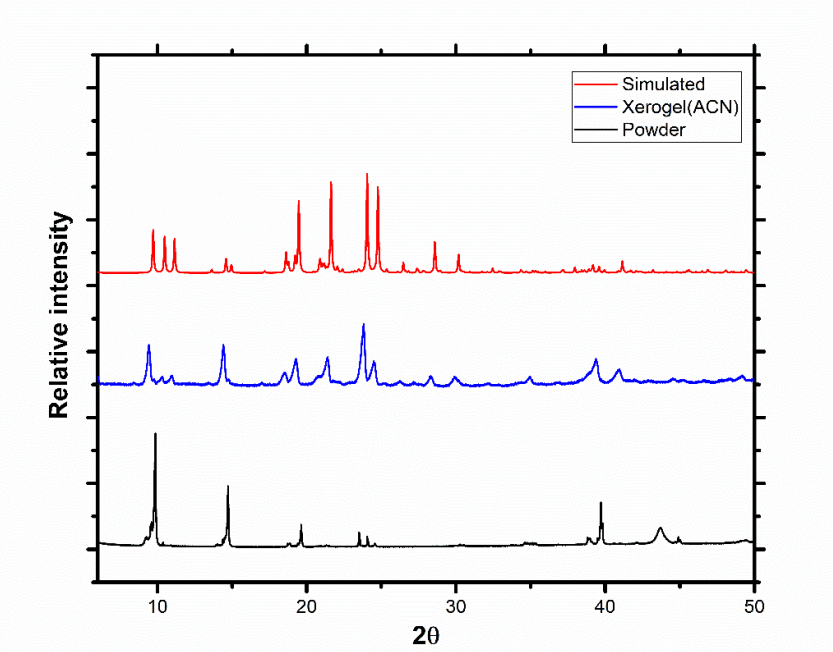

Figure 2.11 *Comparison of PXRD pattern of Powder, Xerogel(crystal) and simulated of Tz-9.*

Whereas, PXRD pattern of xerogel obtained from ACN displayed d-spacings values lower than PXRD of bulk solid suggested better packing in the xerogel state. Specifically, an intense peak at 23.81˚ (d = 3.73 Å) is found to be matching with the distance between two dimeric molecules stacking distance between two molecules of **Tz-9** and d-spacing of 2.28 Å matches well with the distance between two molecules forming dimer (see Figure 2.12).

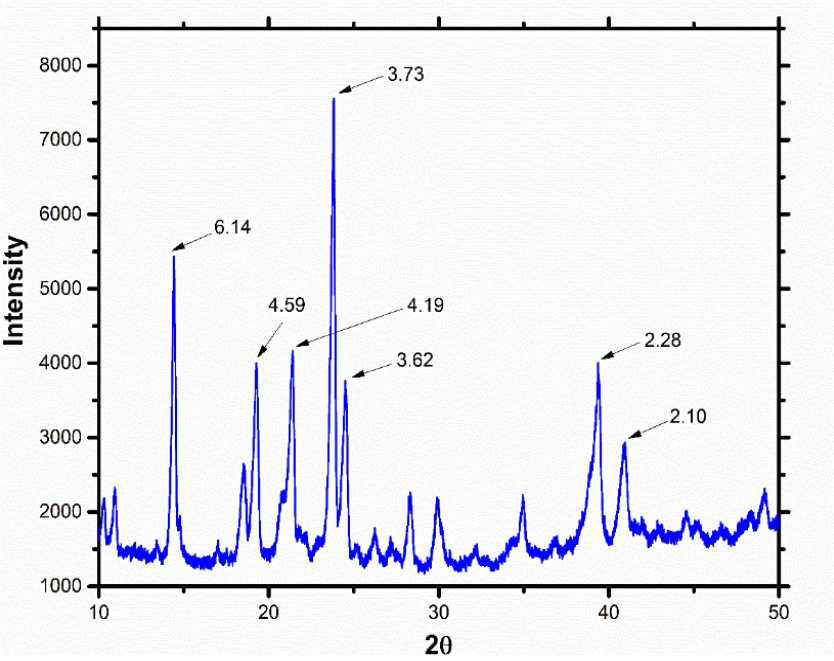

Figure 2.12 *PXRD pattern of xerogel(crystal)*

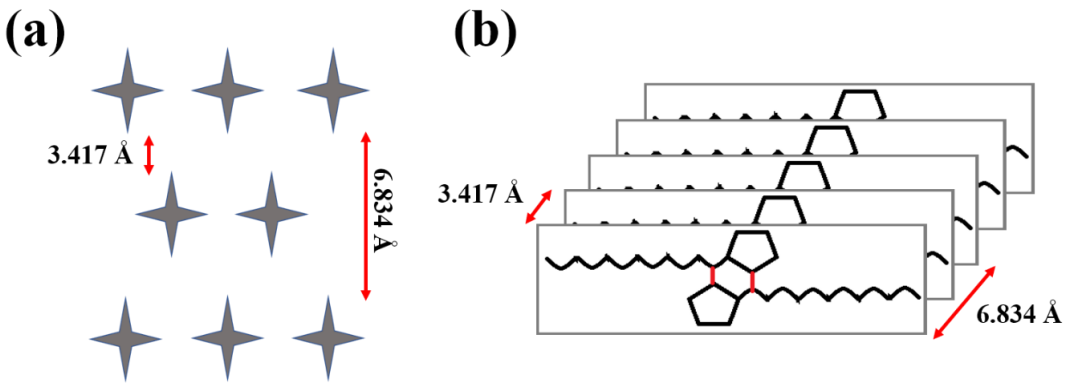

Scheme 2.3 *Cartoon representation (a)Side view of network representing "Brickwall Motif" (b) side view of 3D network representing "Molecular Staircase"*

Furthermore, peak at 14.4 ° (d = 6.14 Å) is close to the distance between the alternate molecule in the bricked structure (Scheme 2.3a). and peak at 4.59 Å is close to the alkyl -alkyl chain distance in the single crystal structures. Thus, it can be proposed that the two dimers are forming the plane which is connected by the weak van der-Waals forces to form 3D network to entrap the solvent. SAXS technique is widely used to obtain information of nanometer to micrometer level structure. Furthermore, as gelator molecule consist of fiber network, this technique is usually utilized for the shape, size and distribution of this fibers[47]. SAXS experiments was performed on the solid samples (figure 2.13-2.15) and their parameter was summarized in the table 2.4. Almost all the samples show the mixture of two or more crystalline structures.

Table 2.4 *Structural parameters obtained from SAXS data.*

Sr.No.	Compound	Space group	Lattice parameter (Å)	Remarks
1	Tz-9	Pm3n	36.8	Only two peaks at q=0.24 $Å^{-1}$ &q=0.33 $Å^{-1}$
2	Tz-10	Lamellar	21.1	Additional few peaks at q=0.12 $Å^{-1}$, q=0.25 $Å^{-1}$ & q=0.28 $Å^{-1}$
3	Tz-11	Lamellar	20.5	Additional peaks at q=0.21 $Å^{-1}$ & q=0.63 $Å^{-1}$
4	Tz-12	Lamellar	23.4	Additional few peaks at q=0.15 $Å^{-1}$, q=0.24 $Å^{-1}$ & q=0.26 $Å^{-1}$
5	Tz-14	Lamellar	104.7 & 26.0	Few additional peaks shown in figure
6	Tz-16	Lamellar	25.4	Additional peak at q=0.16 $Å^{-1}$

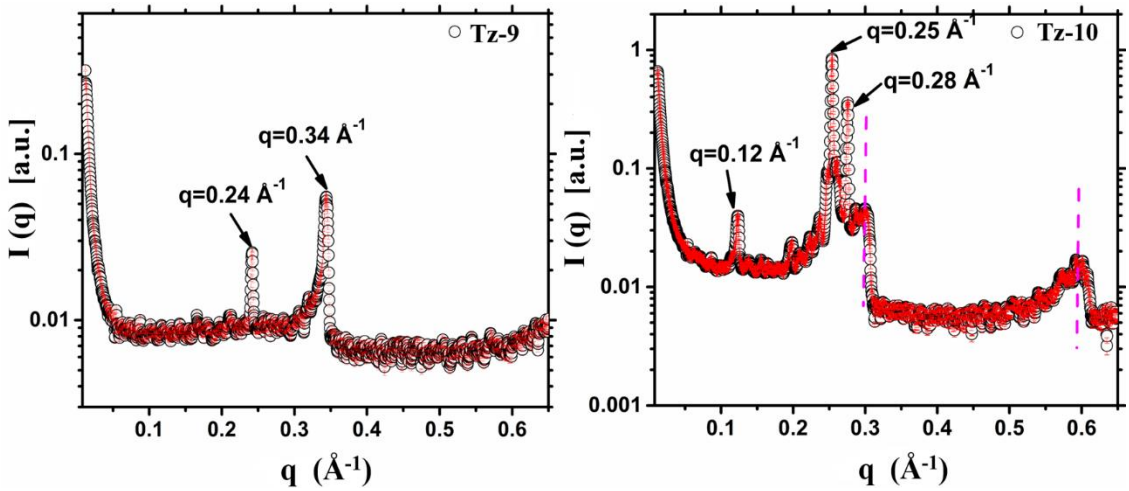

Figure 2.13 *SAXS pattern of Tz-9 and Tz-10*

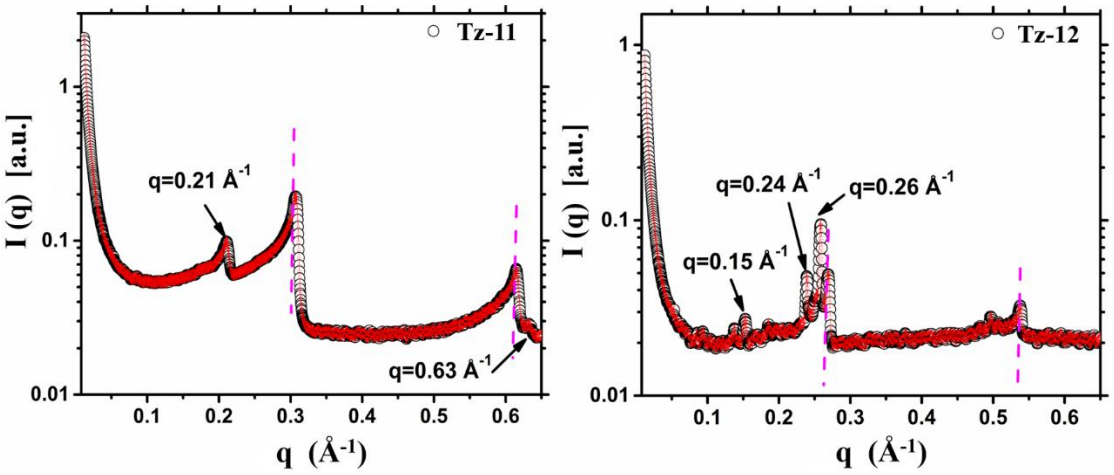

Figure 2.14 *SAXS pattern of Tz-11 and Tz-12*

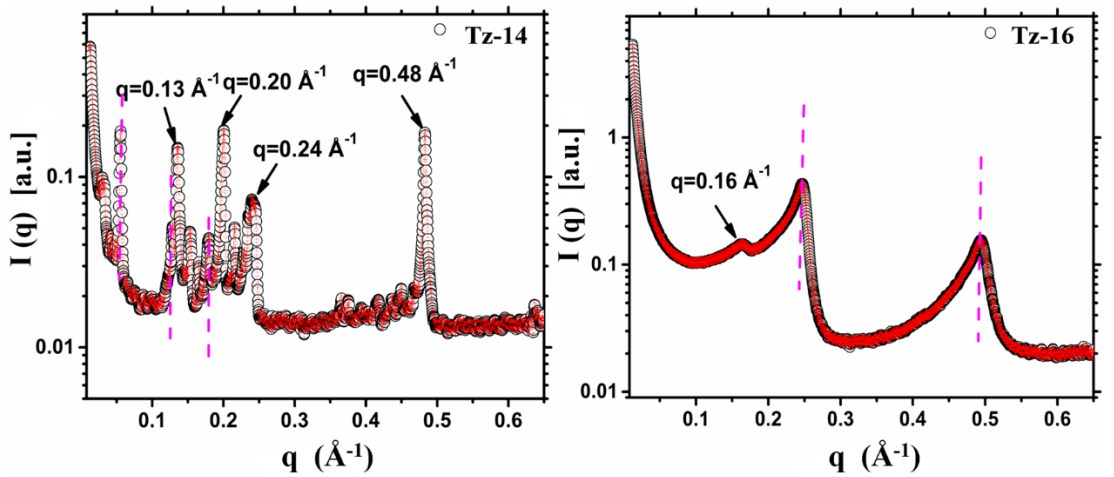

Figure 2.15 *SAXS pattern of Tz-14 and Tz-16*

2.4.6 Small angle neutron scattering (SANS) studies

SANS study was carried out to select the best molecules from the list of molecules Tz-9 to Tz-12, Tz-14, Tz-16 to study the hierarchical assembly of molecules from solid-state to semi-solid gel state.

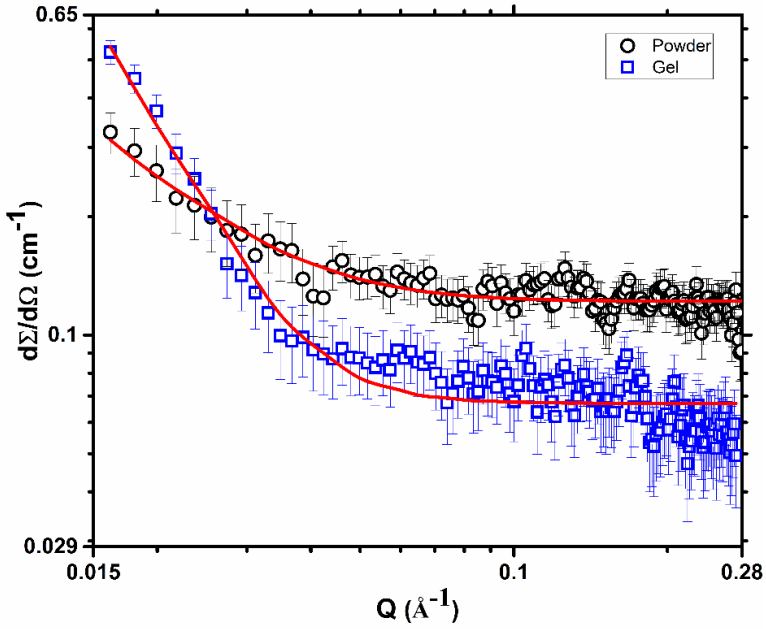

Figure 2.16 *Fitted SANS profile for compound Tz-9. Open circle represents the gel and open square represents native solid where red solid lines represent the fit to the data*

The preliminary study of solid-state study of thiazole-based amide suggested a well-defined cylindrical assembly in solid-state (in Tz-9) (figure 2.16) whereas other synthesized molecules lack cylindrical packing in the solid-state i.e., Tz-10 to Tz-12, Tz-14 and Tz-16, and displayed a less precise laminar packing. **Tz-9** molecule were selected for a detailed study of molecular packing in the crystalline phase to packing in the gel phase in acetonitrile. SANS analysis of gel sample of **Tz-9** was carried out with a gradual change in temperature(figure 2.17), a dependable method to probe the assembly of molecules in the gel phase and to understand the change in assembly, especially at sol-gel transition temperature[48–50]. Therefore, a temperature dependent study of gel sample of **Tz-9** in ACN was undertaken to understand the change in shape and size of molecular fibers in gel phase and in sol phase. Moreover, the effort was also directed to find a correlation between the packing of the molecule in solid-state and packing in the gelator fibers. We believe the present study represents a novel finding between the packing of molecules directly from the thermodynamically stable crystalline phase to the metastable gel phase.

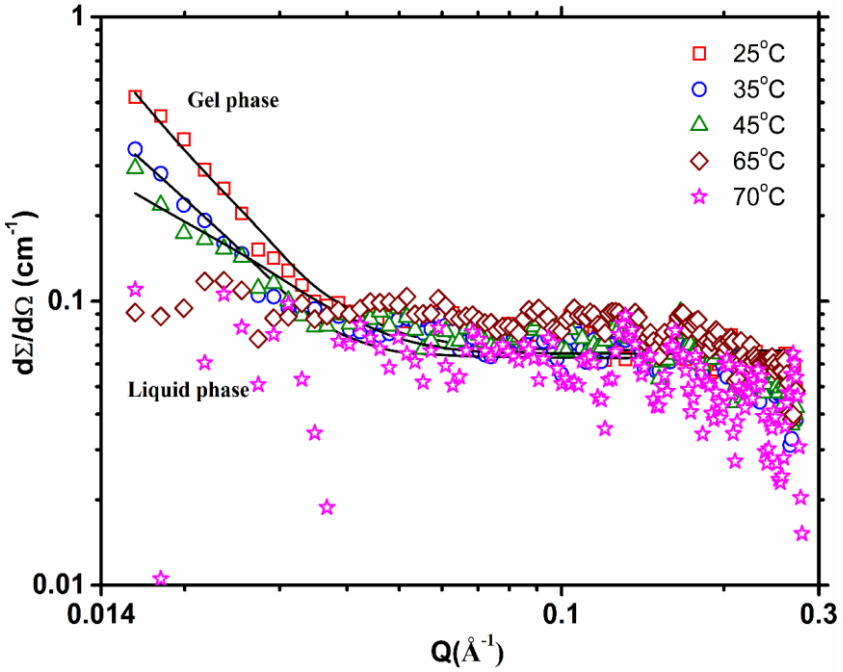

Figure 2.17 *SANS profile of Acetonitrile gel of Tz-9 at different temperature where solid lines represent best possible fitting where black solid lines represents fit to the data*

The scattering profile of solid (open square) and native gel state (open circle) at 25 °C in the deuterated ACN as deuterated solvents ensure good contrast between fibers and the solvent molecule[51] (Figure 2.16). In this figure, solid lines represent the best possible fitting using a model with monodisperse cylindrical form factor. The radius of the cylinder assembly was calculated to be 43.8 Å (in solid-state) and 84.1 Å (in gel state) which is almost double. It is to be noted that the length of the fibers calculated from the scattering is limited by the maximum length accessible by the instrument. The higher value of the cross-sectional radius of cylindrical assembly in the gel phase may be attributed to further association of molecular fibers through multiple C–H···O and van der Waals interactions.

Table 2.5 *Fitted parameters obtain from SANS analysis*

Nature of Tz-9	Temperature (˚C)	Cross sectional radius (R_{cr})	Length of cylinder(L)
Solid	25	43.8 Å	>350 Å
Gel	25	84.1 Å	>350 Å
Gel	35	80.2 Å	>350 Å
Gel	45	55.2 Å	>350 Å
Solution	65	-	-
Solution	70	-	-

Furthermore, to probe the change of shape and size of cylindrical assembly with gel-sol transition in acetonitrile gel of **Tz-9**, temperature dependent SANS study was

carried out (Figure 2.16). Interestingly, the SANS profiles for gel at different temperatures (25°C–45°C) show the same shape in log-log plot with a gradual decrease in the intensity with an increase in the temperature (upto 45 °C), and drastic decrease in scattering intensity above 45 °C. In the fitting analysis, we obtained the value of mean cross-sectional radii of the fibers (Table 2.5).

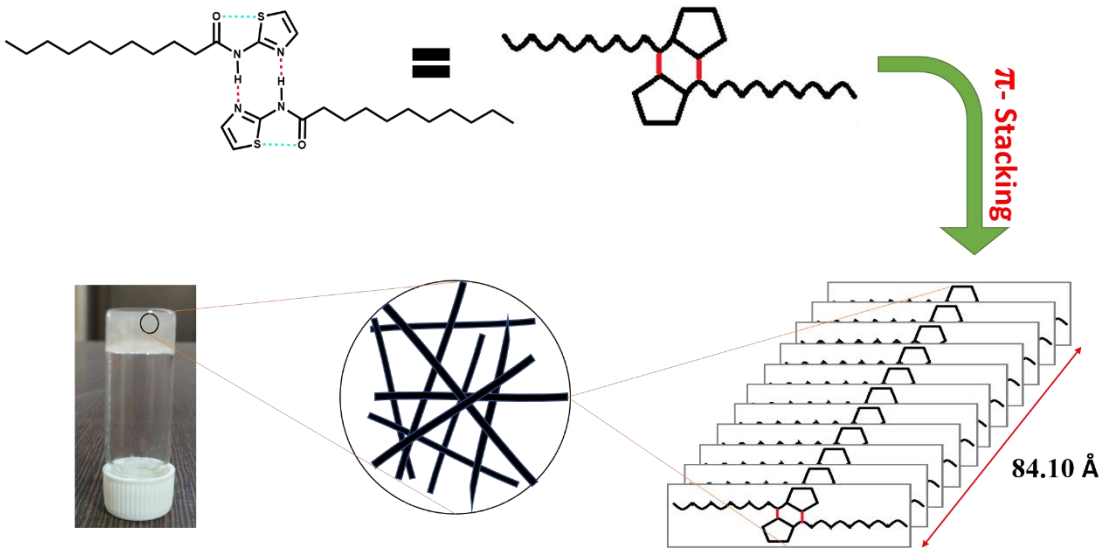

Scheme 2.4 *Cartoon representation for Probable mechanism of gelation of Tz-9*

Understandably, crystalline cylindrical fibers present in the gel network dissociate into less packed cylindrical fibers (low cross-sectional radii) with increase in temperature. The SANS analysis of Tz-9 in ACN gel above gel-sol transition temperature (T_{gel}) i.e. 65 °C and above, show insignificant scattering suggested the complete break-down of supramolecular assembly of gelator fibers into molecule fibers (Fig. 2.16).We propose a probable mechanism of formation of gelator fibers of Tz-9 molecules in ACN from solid-state crystalline packing to semisolid gel assembly based on the results obtained from single crystal XRD, FT-IR, Powder XRD, SEM and SANS analysis (Scheme 2.4).

2.4.7 Application of Tz-9 molecules as Fluoride (F^-) anion sensor

In search of the potential application of **Tz-9** compound, we realized that amide functionality and multiple hydrogen bonding sites present in the molecule may induce anion sensing property[52–54]. Anion sensing property of **Tz-9** was explored in the presence of three anions, namely, fluoride(F^-), dihydrogenphosphate ($H_2PO_4^{2-}$), bromide (Br^-) in tetrahydrofuran (THF) at RT (25 °C). The solution of Tz-9 was titrated with the tertiary butylammonium salt of various anions. Interestingly, THF solution of

Tz-9 selectively binds with fluoride(F^-) over $H_2PO_4^{2-}$ and Br^- as evident from significant red shift in UV–vis signal (Figure 2.18).

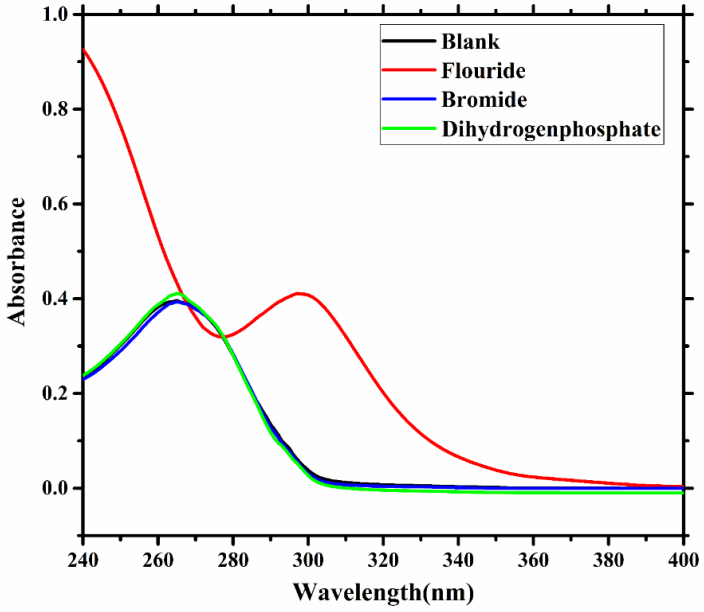

Figure 2.18 *Absorption spectra of compound Tz-9 (6 μM) in absence and presence of 1.0 equivalent of F^-, Br^- and $H_2PO_4^-$ anions in THF*

UV-Visible absorbance peak of Tz-9 was observed at 265 nm (in blank) which was red-shifted to the 300 nm (with F^-) ion. This significant shift in absorbance wavelength (35 nm) with F^- and no change with the other two ions suggest a preferential recognition of fluoride ion (Figure 2.19).

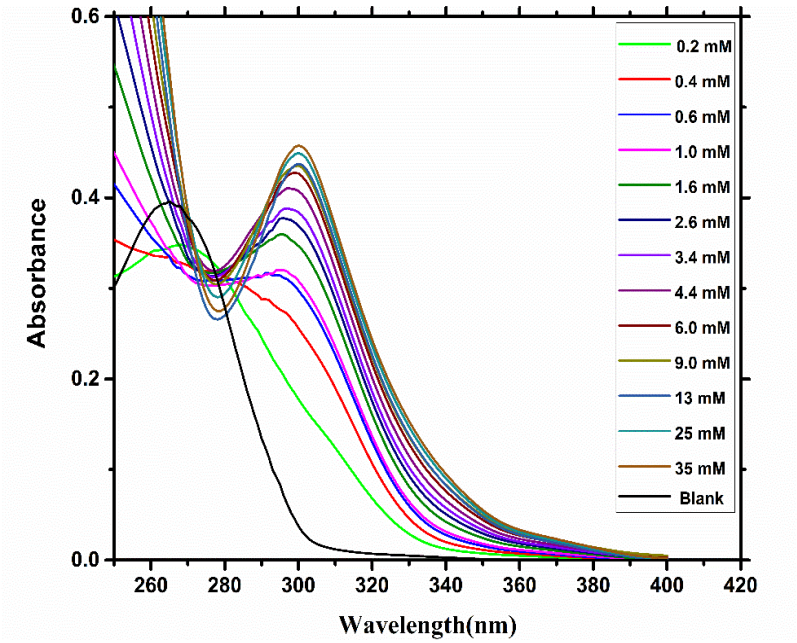

Figure 2.19 *Absorption spectra changes with the addition of TBAF (0-35 μM) in THF*

The Fluorescence emission spectra of compound **Tz-9**(Figure 2.20), upon the addition of TBAF (0-35 μM) excited at 265 nm and emission at 311 nm, displayed significant decreases in fluorescence (10-fold) with an increase in the fluoride ion concentration (up to 6 equivalent).

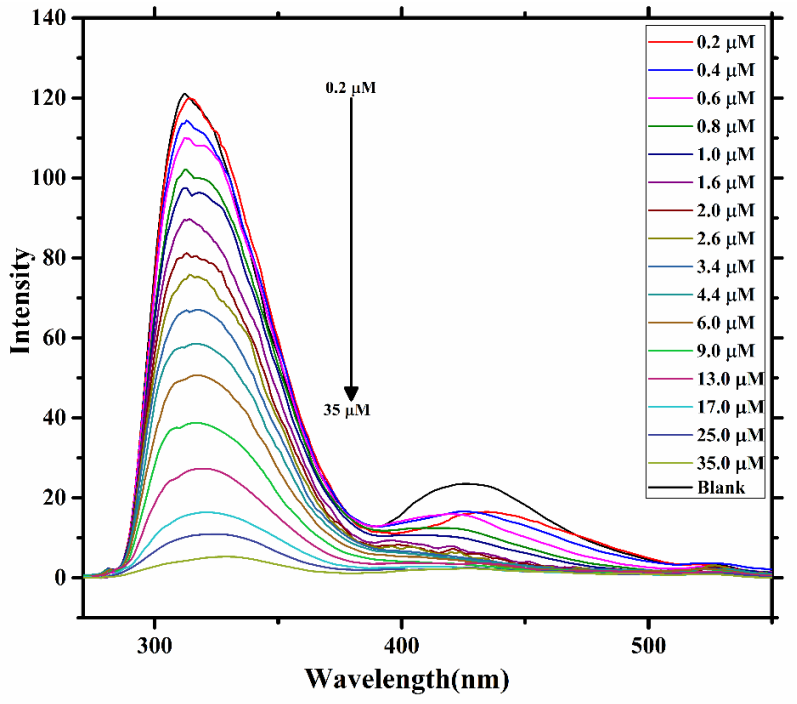

Figure 2.20 *Fluorescence emission spectra of compound Tz-9(6 μM) upon addition of TBAF*

Therefore, **Tz-9** molecule in THF can selectively and effectively binds with F^- ion at very low concentration even in presence of other competing anions and may find application as sensor. Recently, Young Ju Lee et. al.[55] demonstrated fluoride ion effect on sol-gel transition of hydrazide based organogelator and naked eye visualization of phase transition with fluoride ion addition. In order to explore the effect of fluoride ion on sol-gel phase transition of **Tz-9** gel in acetonitrile, we performed similar experiments with **Tz-9** gelator in acetonitrile. Surprisingly, we observed no visual effect of fluoride ion on gel formation or sol-gel phase transition of **Tz-9** gel in acetonitrile. However, it suggests the retention of supramolecular assembly of **Tz-9** molecules inside the gel fibers even in the presence of fluoride ion. We propose that the carbonyl oxygen of amide functionality of **Tz-9** is forming weak bond with F^- ion. As carbonyl oxygen of amide group of **Tz-9** is forming intramolecular bond with sulphur atom of thiazole moiety (S···O) and not forming strong hydrogen bond such as N-H····O with neighbouring molecules of **Tz-9** (as observed in the single crystal structure).

We believe lone pair of electrons of oxygen atom of carbonyl functionality is readily available to bind with F ion without disturbing the overall hydrogen bonded network required for formation of 3-D network of gel. Appearance of a strong absorbance maxima corresponding to n→π* at 300 nm after addition of fluoride ion to **Tz-9** solution in THF further support our hypothesis.

2.5 Conclusions

We prepared a series of thiazole-based amide with different aliphatic chain length (Tz-**9** to Tz-12, Tz-15 and Tz-16) and decided to explore the packing of molecules from crystalline state to semi-solid gel. A simple strategy to record the SANS and SAXS data of solid sample of the synthesized compound, before subjecting the samples for extensive analysis, resulted in the selection of promising candidate i.e., **Tz-9** molecules. **Tz-9** molecules, even in crystalline state, displayed well defined cylindrical packing, whereas other thiazole amide-based compounds have lamellar packing. The selected compound **Tz-9** was further examined for its gelation property and turned out to be an excellent gelator for polar solvent with low MGC for acetonitrile gel (2.78 (% w/v)). Temperature dependent SANS study of **Tz-9** gel in acetonitrile suggested the three-dimensional network of gel is primarily consisting of monodisperse cylindrical fibers with almost the double molecular diameter than the cylindrical fibers in the solid state. Moreover, the decrease in molecular diameter of cylindrical fibers in gel network with increase in temperature and complete collapse of cylindrical assembly at higher temperature (70 °C) was evident from temperature dependent SANS study. Single crystal structure of Tz-9 packing displayed dimeric zero-dimensional packing of the molecule with the extended aliphatic chain which was extended further to 2D network through weak noncovalent interactions such as C–H···O and van der Waals interaction. A probable mechanism of packing of **Tz-9** molecules starting from solid state to supramolecular assembly inside the gelator fiber is proposed based on various physical-chemical analysis. A potential application of **Tz-9** as Fluoride ion sensing with good selectivity and sensitivity may open an avenue to develop as sensors.

References

1. Abdallah, D. J. & Weiss, R. G. Organogels and low molecular mass organic gelators. *Adv. Mater.* **12**, 1237–1247 (2000).
2. Terech, P. & Weiss, R. G. Low molecular mass gelators of organic liquids and the properties of their gels. *Chem. Rev.* **97**, 3133–3159 (1997).
3. Lan, Y., Corradini, M. G., Weiss, R. G., Raghavan, S. R. & Rogers, M. A. To gel or not to gel: correlating molecular gelation with solvent parameters. *Chem. Soc. Rev.* **44**, 6035–6058 (2015).
4. Estroff, L. A. & Hamilton, A. D. Water gelation by small organic molecules. *Chem. Rev.* **104**, 1201–1217 (2004).
5. Sangeetha, N. M. & Maitra, U. Supramolecular gels: Functions and uses. *Chem. Soc. Rev.* **34**, 821–836 (2005).
6. Piepenbrock, M. M., Lloyd, G. O., Clarke, N. & Steed, J. W. Metal- and Anion-Binding Supramolecular Gels. *Chem. Rev.* **110**, 1960–2004 (2010).
7. Van Bommel, K. J. C., Stuart, M. C. A., Feringa, B. L. & Van Esch, J. Two-stage enzyme mediated drug release from LMWG hydrogels. *Org. Biomol. Chem.* **3**, 2917–2920 (2005).
8. Jadhav, S. R., Vemula, P. K., Kumar, R., Raghavan, S. R. & John, G. Sugar-derived phase-selective molecular gelators as model solidifiers for oil spills. *Angew. Chemie - Int. Ed.* **49**, 7695–7698 (2010).
9. Vibhute, A. M., Muvvala, V. & Sureshan, K. M. A Sugar-Based Gelator for Marine Oil-Spill Recovery. *Angew. Chemie - Int. Ed.* **55**, 7782–7785 (2016).
10. Yasuda, Y., Kamiyama, T. & Shirota, Y. Ionic conductivities of low molecular-weight organic gels and their application as electrochromic materials. *Electrochim. Acta* **45**, 1537–1541 (2000).
11. Smith, D. K. Dendritic supermolecules - Towards controllable nanomaterials. *Chem. Commun.* 34–44 (2006).
12. Sivakova, S. & Rowan, S. J. Nucleobases as supramolecular motifs. *Chem. Soc. Rev.* **34**, 9–21 (2005).
13. Gronwald, O. & Shinkai, S. Sugar-Integrated Gelators of Organic Solvents. *Chem. - A Eur. J.* **7**, 4328–4334 (2001).
14. Babu, S. S., Praveen, V. K. & Ajayaghosh, A. Functional π-gelators and their applications. *Chemical Reviews* **114**, 1973–2129 (2014).
15. Yamanaka, M. Urea derivatives as low-molecular-weight gelators. *J. Incl. Phenom. Macrocycl. Chem.* **77**, 33–48 (2013).
16. George, M., Tan, G., John, V. T. & Weiss, R. G. Urea and thiourea derivatives as low molecular-mass organogelators. *Chem. - A Eur. J.* **11**, 3243–3254 (2005).
17. Suzuki, M. & Hanabusa, K. L-Lysine-based low-molecular-weight gelators. *Chem. Soc. Rev.* **38**, 967–975 (2009).
18. Adams, D. J. Dipeptide and Tripeptide Conjugates as Low-Molecular-Weight Hydrogelators. *Macromol. Biosci.* **11**, 160–173 (2011).
19. Estroff, L. A. & Hamilton, A. D. Water gelation by small organic molecules. *Chem. Rev.* **104**, 1201–1217 (2004).
20. Yu, G., Yan, X., Han, C. & Huang, F. Characterization of supramolecular gels. *Chem. Soc. Rev.* **42**, 6697–6722 (2013).
21. Yadav, P. & Ballabh, A. Odd-even effect in a thiazole based organogelator: Understanding the interplay of non-covalent interactions on property and applications. *New J. Chem.* **39**, 721–730 (2015).

22. Yadav, P., Kour, D., Gupta, V. K., Rajnikant & Ballabh, A. Probing the role of weaker interactions in immobilization of solvents in a new class of supramolecular gelator. *RSC Adv.* **3**, 8417–8421 (2013).
23. Yadav, P., Dutta, P. K. & Ballabh, A. Combinatorial library approach to realize 2-aminothiazole-based two-component hydrogelator: A structure - Property correlation. *Crystal Growth and Design* **14**, 5966–5975 (2014).
24. Yadav, P. & Ballabh, A. Room temperature metallogelation for a simple series of aminothiazole ligands with potential. *RSC Adv.* **4**, 563–566 (2014).
25. Rosa Nunes, D. *et al.* Organogel Formation Rationalized by Hansen Solubility Parameters: Shift of the Gelation Sphere with the Gelator Structure. *Langmuir* **35**, 7970–7977 (2019).
26. Spackman, M. A. & Jayatilaka, D. Hirshfeld surface analysis. *CrystEngComm* **11**, 19–32 (2009).
27. Dolomanov, O. V., Bourhis, L. J., Gildea, R. J., Howard, J. A. K. & Puschmann, H. OLEX2: A complete structure solution, refinement and analysis program. *J. Appl. Crystallogr.* **42**, 339–441 (2009).
28. Sheldrick, G. M. Crystal structure refinement with SHELXL. *Acta Crystallogr. Sect. C Struct. Chem.* **71**, 3–8 (2015).
29. Sheldrick, G. M. A short history of SHELX. *Acta Crystallogr. Sect. A Found. Crystallogr.* **64**, 112–122 (2008).
30. Aswal, V. K. & Goyal, P. S. Small-angle neutron scattering diffractometer at Dhruva reactor. *Curr. Sci.* **79**, 947–953 (2000).
31. Singh, O., Kaur, R., Aswal, V. K. & Mahajan, R. K. Composition and Concentration Gradient Induced Structural Transition from Micelles to Vesicles in the Mixed System of Ionic Liquid-Diclofenac Sodium. *Langmuir* **32**, 6638–6647 (2016).
32. Kaur, R., Kumar, S., Aswal, V. K. & Mahajan, R. K. Influence of headgroup on the aggregation and interactional behavior of twin-tailed cationic surfactants with pluronics. *Langmuir* **29**, 11821–11833 (2013).
33. Hayter, J. B. & Penfold, J. Determination of micelle structure and charge by neutron small-angle scattering. *Colloid Polym. Sci.* **261**, 1022–1030 (1983).
34. Kaler, E. W. Small-angle scattering from colloidal dispersions. *J. Appl. Crystallogr.* **21**, 729–736 (1988).
35. Pedersen, J. S. Analysis of small-angle scattering data from colloids and polymer solutions: Modeling and least-squares fitting. *Adv. Colloid Interface Sci.* **70**, 171–210 (1997).
36. Andre Guinier. *Small- angle Scattering of X-rays*. (Wiley-VCH, 1955).
37. Richard G. Weiss, P. T. *Molecular gels: Material with self-assembled fibrillar network*. (Springer Dordrecht, 2006).
38. Das, U. K., Trivedi, D. R., Adarsh, N. N. & Dastidar, P. Supramolecular synthons in noncovalent synthesis of a class of gelators derived from simple organic salts: Instant gelation of organic fluids at room temperature via in situ synthesis of the gelators. *J. Org. Chem.* **74**, 7111–7121 (2009).
39. Ballabh, A., Adalder, T. K. & Dastidar, P. Structures and gelation properties of a series of salts derived from an alicyclic dicarboxylic acid and n-alkyl primary amines. *Cryst. Growth Des.* **8**, 4144–4149 (2008).
40. Higashi, A., Czarnecki, M. A. & Ozaki, Y. Infrared study of solids and cast films of long-chain fatty acids. *Thin Solid Films* **230**, 203–208 (1993).
41. Vishweshwar, P., Nangia, A. & Lynch, V. M. Pyrazine-2,3-dicarboxamide. *Acta Crystallogr. Sect. C Cryst. Struct. Commun.* **56**, 1512–1514 (2000).

42. Feast, W. J., Lövenich, P. W., Puschmann, H. & Taliani, C. Synthesis and structure of 4,4′-bis(2,3,4,5,6-pentafluorostyryl)stilbene, a self-assembling J aggregate based on aryl-fluoroaryl interactions. *Chem. Commun.* 505–506 (2001).
43. Ostuni, E., Kamaras, P. & Weiss, R. G. Novel x-ray method for in situ determination of gelator strand structure: Polymorphism of cholesteryl anthraquinone-2-carboxylate. *Angew. Chemie (International Ed. English)* **35**, 1324–1326 (1996).
44. Jung, J. H. *et al.* Self-assembly of a sugar-based gelator in water: Its remarkable diversity in gelation ability and aggregate structure. *Langmuir* **17**, 7229–7232 (2001).
45. Yan, N., He, G., Zhang, H., Ding, L. & Fang, Y. Glucose-based fluorescent low-molecular mass compounds: Creation of simple and versatile supramolecular gelators. *Langmuir* **26**, 5909–5917 (2010).
46. George, M. & Weiss, R. G. Chemically reversible organogels via 'latent' gelators. Aliphatic amines with carbon dioxide and their ammonium carbamates. *Langmuir* **18**, 7124–7135 (2002).
47. Yu, G., Yan, X., Han, C. & Huang, F. Characterization of supramolecular gels. *Chem. Soc. Rev.* **42**, 6697–6722 (2013).
48. Nostro, P. Lo *et al.* Organogels from a vitamin C-based surfactant. *J. Phys. Chem. B* **111**, 11714–11721 (2007).
49. Morris, K. L. *et al.* Chemically programmed self-sorting of gelator networks. *Nat. Commun.* **4**, 1–6 (2013).
50. George, M., Snyder, S. L., Terech, P., Glinka, C. J. & Weiss, R. G. N-alkyl perfluoroalkanamides as low molecular-mass organogelators. *J. Am. Chem. Soc.* **125**, 10275–10283 (2003).
51. Sahoo, P. *et al.* Combinatorial library of primaryalkylammonium dicarboxylate gelators: A supramolecular synthon approach. *Langmuir* **25**, 8742–8750 (2009).
52. Amendola, V., Esteban-Gómez, D., Fabbrizzi, L. & Licchelli, M. What anions do to N-H-containing receptors. *Acc. Chem. Res.* **39**, 343–353 (2006).
53. Cidalia M. G. dos Santos, Thomas McCabe, Graeme W. Watson,†, P. E. K. and T. G. The Recognition and Sensing of Anions through " Positive Allosteric Effects " Using Simple Urea - Amide Receptors. *J. Org. Chem.* **73**, 9235–9244 (2008).
54. Wenzel, M., Hiscock, J. R. & Gale, P. A. Anion receptor chemistry: Highlights from 2010. *Chem. Soc. Rev.* **41**, 480–520 (2012).
55. Park, S., Ju, J., Lee, Y. J. & Lee, S. Y. A hydrazide organogelator for fluoride sensing with hyperchromicity and gel-to-sol transition. *RSC Adv.* **10**, 14243–14248 (2020).